Bond-valence analysis on the structural effects in magnetoresistive manganese perovskites

1998 J. Phys.: Condens. Matter 10 L757

(http://iopscience.iop.org/0953-8984/10/48/001)

J. Phys.: Condens. Matter **10** (1998) L757–L763. Printed in the UK PII: S0953-8984(98)97792-X

LETTER TO THE EDITOR

Bond-valence analysis on the structural effects in magnetoresistive manganese perovskites

G H Rao†‡, K Bärner† and I D Brown§

† IV Physikalisches Institut der Universität Göttingen, Bunsenstrasse 11–15, D-37073 Göttingen, Germany

‡ Institute of Physics and Centre for Condensed Matter Physics, Chinese Academy of Sciences, Beijing 100080, People's Republic of China

§ Brockhouse Institute for Materials Research, McMaster University, Hamilton, Ontario, Canada L8S 4M1

Received 23 September 1998

Abstract. For the $AMnO_3$ perovskites that show colossal-magnetoresistance (CMR) behaviour, we use the global instability index, $R1$, as a measure of the influence of the static lattice effects on the magnetic and electrical properties. These effects arise from the size mismatch between the ions at A and Mn sites as well as the size distribution of ions at A sites. A magnetic and electronic phase diagram as a function of $R1$ for $R_{0.7}A'_{0.3}MnO_3$ (R = trivalent rare-earth ions, A′ = divalent alkaline-earth ions) reveals four well-defined regions: paramagnetic insulator (PMI), ferromagnetic metal (FMM), spin glass or ferromagnetic insulator (FMI), and a transition region (TMI), in which the compounds exhibit a variety of behaviours.

Manganese perovskites have recently attracted interest because of their colossal-magnetoresistance (CMR) properties and their similarity in both crystal structure and electron correlation behaviours to the high-T_c superconducting cuprates. The simultaneous occurrence of metallic conductivity and ferromagnetism in $R_{1-x}A'_xMnO_3$ compounds (R = trivalent rare-earth ions, A′ = divalent alkaline-earth ions) has long been understood on the basis of the double-exchange (DE) mechanism proposed by Zener [1] and generalized by Anderson and Hasegawa [2] and de Gennes [3]. Both Mn^{3+} and Mn^{4+} have partially filled d shells with strong on-site Hund's coupling, so the Mn t_{2g} electrons provide a local spin of $S = 3/2$ while the Mn^{3+} e_g^1 electron ($S = 1/2$) is itinerant. The ferromagnetic coupling between Mn^{3+} and Mn^{4+} results from the hopping of the e_g electron between Mn^{3+} and Mn^{4+} which in turn is favoured by ferromagnetic ordering since it allows the e_g electrons to hop without a spin flip. However, as pointed out by Millis *et al* [4], the double-exchange mechanism alone cannot explain the electrical and magnetic properties of $R_{1-x}A'_xMnO_3$ compounds, and strong electron–phonon coupling must be taken into account. The electronic and magnetic behaviours of these compounds are essentially controlled by the competition between the double-exchange interaction which favours ferromagnetism and metallic conductivity, an antiferromagnetic interaction which leads to charge localization, and distortions in the chemical structure which tend to localize the charge and hence destroy the ferromagnetic coupling.

There are two important structural effects. The first is the distortion that occurs in the structure as a result of the size mismatch between Mn on the one hand and the R and A′ cations on the other, traditionally measured using the tolerance factor,

0953-8984/98/480757+07$19.50

$t = (r_A + r_O)/\sqrt{2}(r_B + r_O)$ for a perovskite ABO_3. For most of the CMR manganese perovskites $t < 1$, which implies that the cage formed by corner-sharing MnO_6 octahedra is too large for the cations at the A sites, and the structure is distorted by twisting and tilting the MnO_6 octahedra to give the $PrFeO_3$ structure (space group: $Pbnm$) [5]. Such a distortion results in a bending of the Mn–O–Mn bonds, a weakening of the double-exchange interaction, and a reduction of the width of the conduction band, all of which lower the metal–insulator (M–I) transition temperature [6, 7]. The second structural effect is the size and charge difference between the R^{3+} and A'^{2+} cations which, being randomly distributed over the A sites, will cause inhomogeneity in the background potential experienced by the e_g electrons as they move through the crystal, leading to some regions of low potential in which the electrons can be trapped. There are two mechanisms for achieving this. The first is the direct interaction of the electrons with the charges and relaxed environments around the static arrangement of R^{3+} and A'^{2+} cations. This will tend to localize the electrons close to the R^{3+} ion. The second is the dynamic electron–phonon coupling which itself has two components. The first arises from the difference in length between the Mn^{3+}–O and Mn^{4+}–O bonds, a difference which provides a coupling between the electron and the octahedral breathing-mode phonon; the second arises from the Jahn–Teller distortion that occurs around Mn^{3+}, but not around Mn^{4+}, which provides a coupling between the electron and a tetragonal distortion mode of the MnO_6 octahedra. In this letter we consider only the static distortions; the dynamic effects are ignored except to the extent that the static relaxations around the A-site cations may well help to freeze out one or other of these phonons.

A magnetic and electronic phase diagram, showing the transition temperature versus the tolerance factor t, was proposed by Hwang *et al* to represent the static lattice effects due to the size mismatch of cations in $R_{0.7}A'_{0.3}MnO_3$ [8]. In this phase diagram three phase regimes are identified: a paramagnetic insulator (PMI), a ferromagnetic insulator (FMI), and a ferromagnetic metal (FMM) phase. On the PMI/FMM boundary, the Curie temperature (T_c) and M–I transition temperature (T_m) show a maximum at $t = 0.930$ (corresponding to $La_{0.7}Sr_{0.3}MnO_3$).

However, discovery of different transition temperatures for compounds with the same tolerance factor [9, 10] led to the suggestion that the size differences between R^{3+} and A'^{2+} could provide local traps and possibly phase or domain separation [9–13]. Two structural parameters, t, the tolerance factor, and σ^2, the variance of the ionic radius distribution of cations at A sites, were therefore needed to describe the static structural effects that influence the electronic and magnetic properties [9, 14]. Unfortunately, the dimensions of these two quantities are different, making direct comparison difficult. However, the authors of reference [9] showed that, for a given value of t, there was a linear relation between T_m and σ^2: $T_m = T_m(\langle r_A \rangle) - p\sigma^2$, where $T_m(\langle r_A \rangle = 1.23\ \text{Å}) = 400$ K and $p = 20\,600$ K Å^{-2} for $R_{0.7}A'_{0.3}MnO_3$ with $\sigma^2 < 0.015$ Å^2, and they reconstructed the phase diagram of reference [8] in the form of $T_m(\langle r_A \rangle)$ versus $\langle r_A \rangle$ by assuming that p is independent of $\langle r_A \rangle$. Kwon *et al* classified the M–I transition properties of $R_{1-x}A'_xMnO_3$ according to the values of t and σ [14].

In this letter we propose to use a single parameter, $R1$, the global instability index of the bond-valence model [5, 15], to characterize the structural effects arising from both a size mismatch and a size distribution of cations in the CMR manganese perovskites. In the bond-valence model, derived from Pauling's rules, the empirical correlation of equation (1) is used to determine the bond valence, s_{ij}, of a chemical bond from its length, R_{ij}:

$$s_{ij} = \exp\left(\frac{R_0 - R_{ij}}{B}\right) \tag{1}$$

Table 1. The R_0-values used in this work for the bond between a cation and oxygen and the deviation, d_i, from the *valence sum rule* (equation (2)) of the ion in the ideal perovskite structure (see the text).

Ions	La^{3+}	Pr^{3+}	Nd^{3+}	Sm^{3+}	Eu^{3+}	Gd^{3+}	Tb^{3+}	Dy^{3+}	Er^{3+}
R_0	2.172	2.138	2.105	2.090	2.074	2.058	2.032	2.001	1.988
d_i	0.795	0.989	1.160	1.233	1.308	1.380	1.490	1.611	1.659
Ions	Tm^{3+}	Yb^{3+}	Y^{3+}	Ca^{2+}	Sr^{2+}	Ba^{2+}	Mn^{3+}	Mn^{4+}	
R_0	1.978	1.965	2.019	1.967	2.118	2.285	1.760	1.753	
d_i	1.695	1.740	1.542	0.733	0.095	−0.992	0	0	

where $B = 0.37$ and R_0 is the length of a bond of unit valence. The values of R_0 for most of the common bonds are tabulated in reference [16]. The values of R_0 used in the present work for calculating the valence of the bond between a cation and oxygen are listed in table 1.

For most compounds it is found that the sum of the bond valences around any atom, i, is equal (or nearly equal) to its valence or oxidation state, V_i:

$$\sum_j s_{ij} = V_i. \tag{2}$$

In practice equation (2) will rarely be obeyed exactly because of uncertainties in the measured bond length, but the difference between the bond-valence sum and the atomic valence is usually small (<0.1 valence units (v.u.)) unless lattice effects cause excessive stretching or compression of the bonds. Where such lattice strains occur, as they do frequently in the perovskites, it convenient to measure them in terms of the discrepancy, d_i:

$$d_i = V_i - \sum_j s_{ij}. \tag{3}$$

A measure of such lattice strains over the whole structure is the global instability index, $R1$, which is the root mean square average of the d_i-values:

$$R1 = \langle d_i^2 \rangle^{1/2}. \tag{4}$$

Larger values of d_i and $R1$ are indicative of strained bonds which can lead to instabilities in the crystal structure. For unstrained structures $R1 < 0.1$ v.u., but for compounds with lattice-induced strains $R1$ can be as large as 0.2 v.u. Crystal structures with $R1 > 0.2$ v.u. are generally found to be either incorrect or refined in a space group with too high a symmetry [5]. For simple perovskites, $R1$ plays a role similar to that of the tolerance factor, but for perovskites with partial substitution it also includes the destabilizing effects of local inhomogeneities.

In order to compare perovskites with different structures and to keep the calculation of $R1$ simple, we use a cubic reference structure in which all of the Mn–O bonds are of the same length and unstrained, and the Mn–O–Mn angles are 180 degrees. This corresponds to a situation in which the itinerant electrons are not localized on particular Mn atoms, and each Mn atom is treated as having a charge of +3.3 (for $R_{0.7}A'_{0.3}MnO_3$). The Mn–O bond length corresponding to this charge is 1.979 Å (using $R_0 = 0.7R_0(Mn^{3+}) + 0.3R_0(Mn^{4+}) = 1.758$ Å). This is a little larger than the observed Mn–O distance of 1.960 Å found in $R_{2/3}A'_{1/3}MnO_3$ compounds [6] since in the real structure the Mn–O bonds are compressed, but by choosing a reference structure with the larger

distance, d_{Mn} can be set to zero, which simplifies the calculations without altering the relative order of the values of $R1$ for different $R_{0.7}A'_{0.3}MnO_3$ compounds.

With an Mn–O distance of 1.979 Å, the cubic lattice parameter is 3.958 Å and the A–O distance 2.799 Å regardless of the nature of A. From this distance, the values of d_i shown in table 1 can be calculated for each of the possible R^{3+} and A'^{2+} cations using equations (1) and (3). Because the model uses the same size of cell for all compounds, the values of d_i are independent of composition. Table 1 implies that for all A′ and R cations (except Ba^{2+}) the cage in this reference perovskite is too large ($d_i > 0$), so the environment of A-site ions tends to distort to release the internal stresses via rotations of the surrounding MnO_6 octahedrons.

In order to calculate $R1$ for $R_{0.7}A'_{0.3}MnO_3$ it is necessary to make a number of assumptions. The model already assumes that there is no charge localization on the Mn atoms, which simplifies the calculation since $d_{Mn} = 0$. This is permissible because $R1$ is not used to describe the actual state of the structure; it simply serves to order the compounds in a way that indicates which compounds will be more likely to distort and hence become insulating. Charge localization could be included in the calculations, but it would not change the ranking of the different compounds and would only make the calculations more complex. Further assuming that R and A′ are randomly distributed and the structures around R and A′ are independently relaxed, the explicit expression for $R1$ is

$$R1 = [(0.7d^2_{R^{3+}} + 0.3d^2_{A'^{2+}} + 3d^2_{O^{2-}})/5]^{1/2} \tag{5}$$

where $d_{O^{2-}} = (0.7d_{R^{3+}} + 0.3d_{A'^{2+}})/3$ since each O will receive one third of the bonds formed by the A-site cations, 0.7 of those from R^{3+}, and 0.3 of those from A'^{2+}. Since $d_{Mn} = 0$, the Mn–O bonds make no contribution to either $d_{O^{2-}}$ or $R1$. When more than one type of R^{3+} or A'^{2+} atom is present, the term for $d_{R^{3+}}$ or $d_{A'^{2+}}$ must be split into two or more terms.

For all $R_{0.7}A'_{0.3}MnO_3$ compounds investigated in this work, $R1$ falls in the range between 0.335 v.u. ($La_{0.7}Sr_{0.3}MnO_3$) and 0.619 v.u. ($La_{0.2}Y_{0.5}Ca_{0.3}MnO_3$), which is much higher than the critical value of 0.20 v.u. reported as the limit for a stable structure. This implies that the assumed ideal (cubic) perovskite structure is overstrained and will distort to a lower-symmetry structure to release the internal stresses. In fact, all of the CMR $R_{0.7}A'_{0.3}MnO_3$ compounds crystallize in a perovskite structure distorted by rotation of the MnO_6 octahedra to shorten eight or nine of the twelve A–O bonds and to bend the Mn–O–Mn links (space group: $Pbnm$ or $R\bar{3}c$). According to the distortion theorem [5], such a rotation increases the bond-valence sum around R and A′, which will result in $R1$ being smaller for the distorted structure than for the cubic reference structure.

Plotting T_c and T_m against $R1$ leads to the magnetic and electronic phase diagram for $R_{0.7}A'_{0.3}MnO_3$ compounds shown in figure 1. The measured transition temperatures shown in the phase diagrams of references [8, 9] are reproduced in figure 1. The lines show the phase boundaries drawn to fit the properties of $R_{0.7}A'_{0.3}MnO_3$ (data A–E from references [8, 9, 19]), but the points for $R_{1/3}A'_{1/3}MnO_3$ (data F–H from references [12, 17, 18]) also fit equally well. Points corresponding to the compounds with the same $\langle r_A \rangle$ (data C, D from reference [9]) are well separated in this diagram but still fall close to the phase boundaries, showing that $R1$ successfully reproduces the properties of both t and σ.

Besides the three previously identified phase regions: PMI, FMI, and FMM, a new phase region, the transition region (TMI), can be identified in figure 1. A bifurcation of the phase boundary obviously occurs at $R1 \approx 0.45$ v.u. The branch P_2P_3 can be regarded as the extrapolation of the FMM/PMI boundary (P_1P_2). Like the compounds lying on P_1P_2, the compounds lying on P_2P_3 are characterized by a sharp M–I transition

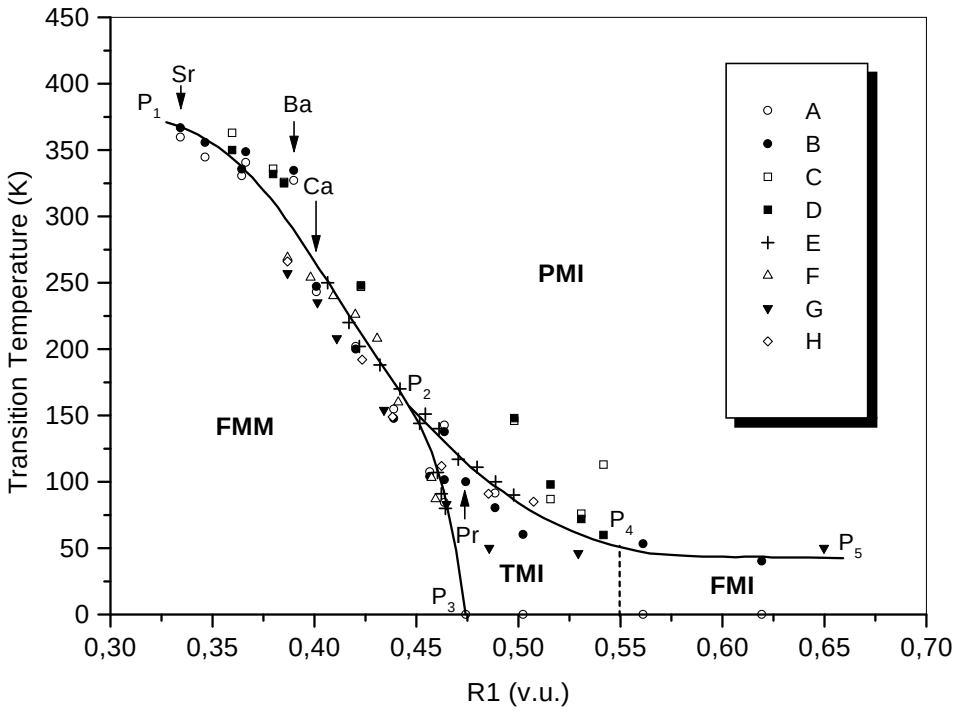

Figure 1. The magnetic and electronic phase diagram of $R_{0.7}A'_{0.3}MnO_3$. The open symbols denote the values of T_m obtained from resistivity measurements, and the (corresponding) closed symbols denote the values of T_c obtained from magnetization measurements. A′ is shown for some typical $La_{0.7}A'_{0.3}MnO_3$ compounds. The data are taken from: reference [8]—A, B (T_c, T_m); reference [9]—C, D (T_c, T_m); reference [19]—E (T_m) ($R_{0.7}A'_{0.3}MnO_3$); reference [12]—F (T_m); reference [17]—G (T_c); reference [18]—H ($R_{2/3}A'_{1/3}MnO_3$) (T_m).

and an almost saturated magnetization at low temperature [19]. The branch P_2P_4 can be regarded as the extrapolation of the FMI/PMI boundary (P_4P_5). However, unlike the compounds lying on P_4P_5, the compounds lying on P_2P_4 may exhibit distinct M–I transitions in the resistivity measurements. The compounds falling in the TMI region are likely to show some instabilities in the magnetic and electronic properties. For instance, $La_{0.7-x}Y_xCa_{0.3}MnO_3$ ($R1 = 0.480$–0.498 v.u.) exhibits a broad M–I transition and a re-entrant semiconducting behaviour as well as a very low magnetization at low temperature [19]. $Pr_{0.7}Ca_{0.3}MnO_3$ ($R1 = 0.474$ v.u.) shows an intriguing charge-ordering instability and a field-induced metamagnetic transition [20]. The last four compounds from reference [9] (data C, D in figure 1), especially $Nd_{0.7}Sr_{0.16}Ba_{0.14}MnO_3$ ($R1 = 0.498$ v.u.), do not fit either the phase diagram of figure 1 or the relationship between T_m and σ^2 proposed in reference [9]. They show a broad or even doubled M–I transition. In particular, $Sm_{0.7}Ba_{0.3}MnO_3$ ($R1 = 0.542$ v.u.) has T_m significantly higher than T_c ($T_m \approx 2T_c$). For $(La_{2/3}Tb_{1/3})_{2/3}Ca_{1/3}MnO_3$ ($R1 = 0.486$ v.u.), neutron diffraction indicated the absence of long-range ferromagnetic ordering but strong short-range magnetic correlations [17]. A spin-glass insulator state sets in for $La_{1-x}Tb_xMnO_3$ with $R1 \geqslant 0.486$ v.u. The TMI/FMI boundary is not well determined from the available data, and we tentatively set it at $R1 = 0.55$ v.u.

The present phase diagram is very similar to that predicted theoretically by Millis

et al [21], except for the existence of the TMI region in figure 1. Both phase diagrams show no maximum on the PMI/FMM boundary ($La_{0.7}Sr_{0.3}MnO_3$ exhibits a higher Curie temperature, T_c, than $La_{0.7}Ba_{0.3}MnO_3$ and $La_{0.7}Ca_{0.3}MnO_3$ because it has a lower $R1$ (=0.335 v.u.) as shown in figure 1). Millis *et al* derived the phase diagram by considering the competition between dynamic Jahn–Teller and the double-exchange effects, and using λ_{eff}, a dimensionless ratio of the self-trapping energy to the effective hopping matrix element, as a characteristic parameter. In fact, one can regard λ_{eff} as a parameter that measures the strength of any phenomenon that damps the double-exchange interaction. Therefore, for the CMR manganese perovskites, $R1$ might be compared to λ_{eff}. However, one has to bear in mind that some entropy effects are considered explicitly in Millis's approach, while the approach proposed in this letter is essentially a method for comparing ground states, i.e. the entropy effects are taken into account implicitly.

Using the hypothetical cubic perovskite as a reference structure, $R1$ provides a measure of the degree of distortion expected for the real structures of $R_{1-x}A'_xMnO_3$ compounds. When $R1$ is small, the lattice strain can be released by small distortions in the real structure, i.e. the real structure is close to the reference structure, and the double-exchange interaction prevails, leading to the simultaneous occurrence of FM–PM and M–I transitions. As $R1$ increases, the different local lattice distortions around A-site ions start to trap the electrons, the double exchange is weakened, and the transition temperature is decreased. When $R1$ is very large, the electrons become trapped and the magnetic ordering breaks down. Many different effects can occur in this region. The weakened magnetic interaction can lead to the formation of paramagnetic or spin-glass insulators such as has been found in $Tb_{2/9}La_{4/9}Ca_{1/3}MnO_3$ [17]. The structure will also be sensitive to the methods of preparation, and phase or domain separation may occur [9, 11–13].

In summary, we have chosen to use $R1$ to measure the expected structural distortion in the real structure that weakens the double exchange in the CMR manganese perovskites, not only because it simultaneously measures the distortions arising from both the mismatch in the size between Mn and the A-site cations as well as the size distribution among the A-site cations themselves, but also because it is easy to calculate and it divides the phase diagram into four cleanly separated regions, FMM, PMI, FMI, and TMI, as shown in figure 1. The compounds falling in the TMI region often exhibit unusual magnetic and electronic properties. For this region, in particular, the details of the electrical and magnetic behaviour must depend on other factors [22] that are not discussed in this letter.

GHR is indebted to the Alexander von Humboldt (AvH) Foundation for a Research Fellowship and to the Chinese Academy of Sciences (CAS) for partial financial aid. KB wishes to acknowledge the continuing support of the Deutsche Forschungsgemeinschaft (DFG). IDB wishes to thank the Natural Science and Engineering Council of Canada for financial support.

References

[1] Zener C 1951 *Phys. Rev.* **82** 403
[2] Anderson P W and Hasegawa H 1955 *Phys. Rev.* **100** 675
[3] de Gennes P-G 1960 *Phys. Rev.* **118** 141
[4] Millis A J, Littlewood P B and Shraiman B I 1995 *Phys. Rev. Lett.* **74** 5144
[5] Brown I D 1992 *Acta Crystallogr.* B **48** 553
[6] García-Muñoz J L, Fontcuberta J, Suaaidi M and Obradors X 1996 *J. Phys.: Condens. Matter* **8** L787
[7] Archibald W, Zhou J-S and Goodenough J B 1996 *Phys. Rev.* B **53** 14 445
[8] Hwang H Y, Cheong S-W, Radaelli P G, Marezio M and Batlogg B 1996 *Phys. Rev. Lett.* **75** 914

[9] Rodriguez-Martinez L M and Attfield J P 1996 *Phys. Rev.* B **54** R15 622
[10] Sun J R, Rao G H and Liang J K 1997 *Appl. Phys. Lett.* **70** 1900
[11] Rao G H, Sun J R, Liang J K, Zhou W Y and Cheng X R 1996 *Appl. Phys. Lett.* **69** 424
[12] Rao G H, Sun J R, Liang J K and Zhou W Y 1997 *Phys. Rev.* B **55** 3742
[13] Rao G H, Sun J R and Liang J K 1997 *J. Appl. Phys.* **82** 4678
[14] Kwon Y U, Chi E O, Kang J K and Hur N H 1997 *J. Appl. Phys.* **82** 3072
[15] Sanches-Salinas A, García-Munoz J L, Rodriguez-Carvajal J, Saez-Puche R and Martinez J L 1992 *J. Solid State Chem.* **100** 201
[16] Brown I D and Altermatt D 1985 *Acta Crystallogr*. B **41** 244
[17] De Teresa J M, Ibarra M R, García J, Blasco J, Ritter C, Algarabel P A, Marquina C and del Moral A 1996 *Phys. Rev. Lett.* **76** 3392
[18] Fontcuberta J, Seffar A, Granados X, García-Muñoz J L, Obradors X and Piñol S 1996 *Appl. Phys. Lett.* **68** 2288
[19] Maignan A, Simon Ch, Caignaert V and Raveau B 1996 *J. Appl. Phys.* **79** 7891
[20] Tomioka Y, Asamitsu A, Kuwahara H, Moritomo Y and Tokura Y 1996 *Phys. Rev*. B **53** R1689
[21] Millis A J, Shraiman B I and Mueller R 1996 *Phys. Rev. Lett.* **77** 175
[22] Liebe J, Kang H, Haupt L, Mandal P, Medvedeva I V, Rao G H, Bärner K *et al* 1998 *J. Appl. Phys.* **83** 7148